European **J**ournal of **Chem**istry

Check for updates

Evaluation of the effects of significant factors and interactions on the enrichment of arsenic and chromium by pipette tip solid phase extraction using novel P-ZrO$_2$CeO$_2$ZnO nanoparticles/alginate beads

Nichodimus Hokonya [iD] 1,*, Courtie Mahamadi [iD] 1,
Netai Mukaratirwa Muchanyereyi [iD] 1 and Timothy Gutu [iD] 2

1 Department of Chemistry, Faculty of Science and Engineering, Bindura University of Science Education, P. Bag 1020 Bindura Zimbabwe
2 Department of Physics, University of Zimbabwe, P.O. Box MP 167 Mount Pleasant Harare, Zimbabwe

* Corresponding author at: Department of Chemistry, Faculty of Science and Engineering, Bindura University of Science Education, P. Bag 1020 Bindura Zimbabwe.
 e-mail: hokonyanichodimus@gmail.com (N. Hokonya).

RESEARCH ARTICLE

KEYWORDS

ABSTRACT

The study seeks to determine the most significant factors affecting arsenic and chromium enrichment using novel P-ZrO$_2$CeO$_2$ZnO nanoparticles/alginate beads in order to minimize the total number of runs needed to successfully run the experiment. The effects of interactions between factors were also evaluated so that the optimum conditions which are not affected by the other factors are chosen for the experiments. The most significant factors on arsenic and chromium enrichment were screened for by using a half-factorial design, followed by the optimization of significant factors using the full-factorial design, and the interaction between factors was determined using ANOVA and interaction plots. The most significant factors for chromium recovery were sample volume, eluent flow rate, and sorbent dosage. For both chromium and arsenic recovery, interactions occurred between sample volume, dosage, and pH. The optimum conditions chosen for the experiment that gave favourable results for both metal ions were sample volume 5 mL, dosage 40 mg, pH = 7 and eluent flow rate 1 mL/min. This study showed that a preliminary screening step for the most significant factors for arsenic and chromium enrichment helps to reduce the number of total runs, and for the same experiment interactions between factors were present; hence, it is necessary to take this into account during the experimental design.

1. Introduction

The heavy metals and metalloids, such as Cd, Cr, Hg, Pb, and As, pollution of water resources have increased the world concern on water pollution in the last decade. These metals do not degrade easily and are highly toxic at low concentrations to aquatic life [1]. The World Health Organization (WHO) has listed some of these metals in the top ten chemicals of public concern [2]. Metalloids such as As have the greatest adverse effects on human health when consumed by drinking contaminated water [3]. In water, As exists in two forms namely As(III) and As(V). As(III) exists under anaerobic conditions in underground water as H_3AsO_3, $H_2AsO_3^-$ and $HAsO_3^{2-}$. As(V) predominates in surface water as H_3AsO_4, $HAsO_3^{2-}$, and H_2AsO^{4-}. Arsenic is used for the production of semiconductors, glass, transistors, paper, pesticides, insecticides, herbicides, and pigments [4]. Long-term exposure of As may result in the development of conjunctivitis, hyperkeratosis, hyperpigmentation, cardiovascular disease, skin cancer, gangrene of limps,

central nervous system disorder, and peripheral vascular system [5].

Chromium is used in alloying, metal ceramic, manufacture of synthetic rubies, dye paints, leather tanning, metal electro-plating, wood preservation, and manufacturing of products for corrosion protection [6]. Cr exists under several oxidation states including II, III, and VI. The divalent Cr species is less abundant due to its instability. Cr(III) is less toxic and has lower solubility as well as mobility and it's an essential micronutrient for many living organisms since it coordinates several amino acid ligands, thereby playing an important role in the metabolism of glucose, lipids and proteins [7]. Cr(VI) is highly soluble, mobile, and strongly oxidizing, resulting in adverse effects on liver, lungs, and kidneys. It is also a potential carcinogenic agent for the respiratory tract [8]. When Cr(VI) is inhaled in excess, it causes lung cancer [9].

Trace element analysis of heavy metals is important for the monitoring and identification of health problems. Various techniques have been applied for the determination of trace metals, including Flow Injection Analysis Atomic Adsorption

Spectrometry (FIA-AAS), Electrothermal Atomic Absorption Spectrometry (ETAAS), Inductively Coupled Plasma Mass Spectrometry (ICP-MS), Atomic Fluorescence Spectroscopy (AFS), and Inductively Coupled Plasma Optical Emission Spectrometry (ICP-OES) [10]. However, the accuracy, sensitivity, and selectivity of any technique can be improved by preliminary sample preparation, such as enrichment [11]. Trace metals have been enriched using solid phase extraction [12], liquid-liquid microextraction [13,14], cloud point extraction [15], coprecipitation [16], reductive extraction [17], and electrodeposition techniques [18].

Solid-phase extraction is the most commonly used technique for routine analysis of samples because of its low cost, simplicity, rapidity, high preconcentration factors, and low consumption of organic solvents [11]. The performance of solid-phase extraction depends on the properties of the sorbent [19,20]. A wide variety of materials such as activated carbon [21], fibrous TiO2@graphitic carbon nitride nanocomposites [22], graphene-silica hybrids [23] and ionic imprinted polymers [24] have been used as sorbents for solid phase extraction. Nanomaterials have gained popularity as solid phase sorbents for trace elements due to their large surface area and chemical stability [25]. The preconcentration of samples is affected by factors such as sorbent mass, pH, eluent volume, sample volume, and time. Screening of these factors one at a time is tedious, expensive and fail to give information on synergism or antagonism simultaneous contribution on response [26]. Multivariate analysis or chemometrics allows for the optimization of the procedures through fast economic pathways and also for more than one variable to be optimized simultaneously. Multivariate analysis can also provide high quality predictions when studying linear, quadratic and interaction effects which influences a system whereas these interactions are not observed in single factor analysis [27].

In this study, P-ZrO2CeO2ZnO nanoparticles were immobilized on alginate beads and subsequently used for the enrichment of As and Cr from water samples prior to ICP-MS analysis. The experimental variables such as pH, dosage, sample volume, eluent concentration, eluent flow rate were optimized using chemometrics followed by determination of the most significant factors on enrichment and determination of interactions.

2. Experimental

2.1. Chemicals and materials

The leaves of *Flacourtia indica* were harvested in Mtoko district, Zimbabwe (Latitude -17.41, 17° 24' 34.26" S, Longitude 32.22, 32° 13' 30.17 E) during the summer of 2021. The leaves were shade-dried before being ground into a fine powder. The powder was then extracted twice using hot water.

The P-ZrO2CeO2ZnO nanoparticles were fabricated using zirconyl chloride octahydrate (99.5%, Riedel-De-Haen Ag, Germany), zinc nitrate hexahydrate (99.5%, Merck, RSA), cerium (IV) sulphate hydrate, and phosphoric acid (Merck, RSA). The beads were fabricated using P-ZrO2CeO2ZnO nanoparticles, sodium alginate (Sigma Aldrich, USA) and calcium chloride (Saarchem, RSA). The As(III) stock solution was prepared using sodium hydroxide (Glassworld, RSA), arsenic trioxide, and potassium permanganate (Saarchem, RSA). The effect of organic solvents was studied using phenol (91%, Riedel-de-Haen. AG, Switzerland), methanol (Avonchem, UK) and propanol (ACE, RSA). The column was conditioned using nitric acid (Merck, RSA).

As (III) stock solution was prepared by dissolving 1.320 g As_2O_3 in 20 mL of 1.0 M NaOH, to this volume, deionized water was added to increase to 1000 mL. To convert As (III) to As (V), 1 mL of 0.01 M $KMnO_4$ was added to every 2.5 mL of As (III) and stirred for a minute. The solution was left to stand for 24 h and

filtered before use. 1000 ppm Cr (VI) stock solution was prepared by taking 0.275 g of potassium dichromate (Saarchem, RSA) previously dried at 100 °C for one hour and dissolving it in 100 mL of water.

2.2. Instrumentation and conditions

The solid phase extraction (SPE) procedure was performed using a peristaltic pump (Eyela, Model: Microtube MP-3, Japan) attached to a pipette tip loaded with P-ZrO2CeO2ZnO nanoparticles/alginate beads. Elemental analysis was performed using an Agilent ICP-MS 7800 (Agilent Technologies-Australia) with incident RF power: 1550 W, plasma gas flow rate: 15 L/min, replicate analysis: 3, carrier gas flow rate: 1 L/min, tune mode: He, plasma mode: low matrix, machine warmup: 1500 s. The surface properties of the composite were characterized using a Scanning Electron Microscope (Zeiss, Model: Auriga 60), size of composite using Transmission Electron Microscope (Tecnai F20, FEI Company USA), the functional groups of the composite were characterized using Fourier Transform-Infrared Spectrometer (Thermo Fisher Scientific Co., Model: Niolet iS5), surface plasmon resonance using Genesis 10s UV-Vis spectrometer (Thermo-Fisher Scientific Co.), crystallinity was characterised using powder X-ray diffraction (Bruker, Model: D2 Phaser, Germany), Orbital shaker (Griffin, Model: CTR, German), Magnetic stirrer (Stuart Scientific, Model: SM3), the acidity of the solutions was monitored using a pH meter (Adwa, Model: AD1020, Romania), drying oven (Biobase, Model: BOV-V4SF, China) and muffle furnace (Carbolite, Model:OAF 10/1, England). The Brunauer-Emmet-Teller (BET) surface area was also determined by a Tristar II Plus surface and porosity analyser from Micrometrics (USA). Nanoparticle samples were dried at 80 °C for 36 h to remove moisture content prior to analysis. The actual analysis was carried out using an analyser bath temperature of -197.4 °C.

2.3. Synthesis of P-ZrO2CeO2ZnO nanoparticles/alginate composite (NP-ABs)

P-ZrO2CeO2ZnO nanoparticles were synthesised by heating 0.05 M zirconium oxide chloride 8-hydrate, 0.05 M cerium sulphate tetra hydrate, 0.05 M zinc nitrate salts and 4 g per 100 mL *F. indica* leaves extract at pH = 9.0 until there was a homogenous colour change in the suspension. The synthesised NPs were recovered from the suspension by centrifugation. The NPs were dried in an oven at 100 °C and in a muffle furnace at 900 °C to get the solid NPs. The obtained NPs were then immobilized on alginate by mixing 100 mL of 2 % w/v sodium alginate with 4 g P-ZrO2CeO2ZnO NPs using a magnetic stirrer for 4 h at room temperature. 20 mL of 0.1 M calcium chloride was slowly added and the solution stirred on a magnetic stirrer for another 4 h. The extrusion process was carried out using syringes. Curing was done by placing the beads in 2 M calcium chloride solution for 12 h at room temperature. The wet microcapsules were dried in an oven at 60 °C for 24 h to induce shrinking.

### 2.4. Preparation of the recovery test using water samples

The effluent water and well water used for the recovery tests were collected in clean 2 L plastic containers flowed by filtration using a 0.45 µm filter paper and acidified using 1 M HNO_3 followed by storage at 4 °C prior to analysis.

2.5. Solid-phase extraction and recovery procedure

A known amount of NP-ABs was loaded into the pipette tip on top of a small layer of glass wool and the sorbent bed was covered by glass wool.

Table 1. BET surface area analysis of alginate and NP-ABs.

Sample	BET surface area (m²/g)	*t*-Plot micropore area (m²/g)	*t*-Plot external surface area (m²/g)	*t*-Plot micropore volume (cm³/g)
P-ZrO₂CeO₂ZnO NPc	0.4593	0.5090	0.3438	734
Alginate beads	4.3795	2.1577	2.2218	875
1% NP-ABs	7.3302	3.8201	3.5101	162.1
4% NP-ABs	3.3488	4.0670	3.4880	21900
6% NP-ABs	2.0217	2.2540	2.0019	10800
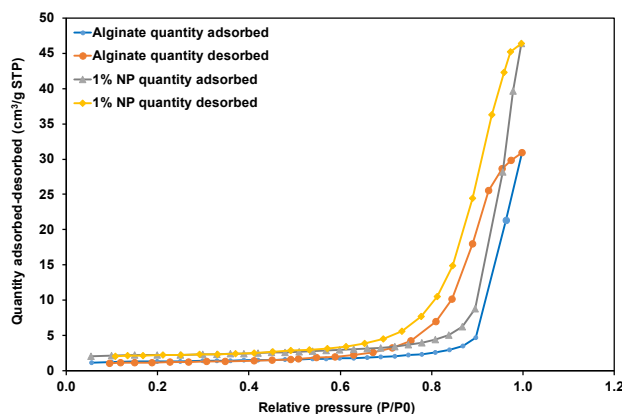
Figure 1. Surface plots for alginate and 1% NP-ABs.

The sorbent bed was conditioned using 1.0 M nitric acid followed by deionized water before use in solid phase experiments at a flow rate of 1 mL/min. A mixture of arsenic and chromium ions was spiked at a concentration of 5 μg/L prepared from ultrapure water. In this study, a screening step was designed using a half-factorial design and Pareto analysis to indicate the variables that are significant for the removal of arsenic and chromium. The optimization step was carried out using an L27 (3^4) Full factorial design matrix. The pH was adjusted to the desired level using nitric acid or sodium hydroxide. An aliquot of the sample was then passed through the column at a flow rate of 1 mL/min. The retained compounds were eluted using nitric acid prior to their determination by ICP-MS. The effect of sample volume was investigated to obtain the highest enrichment factor. Each column experiment was repeated three times to obtain reproducible results.

The removal efficiency (RE %) used to determine the effect of different conditions on adsorption was determined using Equation (1).

$$RE \% = \frac{C_o - C_r}{C_o} \times 100 \tag{1}$$

where C_o and C_r are the initial and residual concentrations of the two metals in solutions in mg/L.

After desorption, the NP-ABs adsorbent was used again for a new cycle of extraction. Extraction recovery (ER) was used to investigate the effect of desorption conditions on the release of metals from the surface of the beads.

The enrichment factor (EF) was determined by calculating the ratio of the concentration of As in the final extract to the initial concentration in the aqueous phase with and without NP-ABs as shown in Equation (2).

$$EF = \frac{C_{des}}{C_0} \tag{2}$$

The extraction recovery (ER %) was determined by the ratio of eluted to initial concentration using Equation (3),

$$ER \% = \frac{C_{des} \times V_{des}}{C_0 \times V_0} \times 100 \tag{3}$$

where C_{des}, C_0, V_{des}, and V_0 are the analyte concentration in the extraction solvent, analyte concentration in the sample, extraction solvent volume and volume of sample.

3. Results and discussion

3.1. Characterization of the prepared NP-ABs material

The amounts of metals incorporated into the NPs and nanoparticles encapsulated into NP-ABs alginate beads were determined by ICP-MS. The amount of zirconia in the NPs was 3458.48 mg/g and the amount incorporated in the 1% NP-ABs was reduced to 360.74 mg/g. 2957.64 mg/g of cerium was present in the NPs, while 395.14 mg/g was incorporated into the 1% NP-ABs. The amount of zinc in the nanoparticles was 6363.2 and 622.73 mg/g was incorporated into the 1% NP-ABs. The results indicate that the nanoparticles were successfully incorporated into the NP-ABs.

The FT-IR spectrum of the free 1% NP-ABs shows a C-O band at 1056 cm⁻¹ [28], and at 1427 cm⁻¹ [29], a H-O-H vibration due to water at 1606 cm⁻¹ and an O-H vibration band at 3332.6 cm⁻¹ [30], a Zn-O stretching band at 425 cm⁻¹ [31], Zr-O band at 494 cm⁻¹ [32]. After As and Cr uptake, the ZrO and ZnO bands do not appear; the C-O bands shift upward and the O-H bands shift downwards, indicating that those bonds participated in the uptake of the metals.

The analysis of Brunauer-Emmet-Teller (BET) surface area was carried out using N₂ adsorption-desorption isotherms for both alginate and NP-Abs, and the results are shown in Table 1 and Figure 1. The surface area, micropore area, and volume of alginate increased when 1% P-ZrO₂CeO₂ZnO nanoparticles were encapsulated, however, upon further increase to 4 and 6 % they decreased. Hence, in this study, the 1% NP-ABs were chosen as the material of choice for the enrichment of As and Cr because of the higher surface area and larger pore volume of the NP-ABs ensure better uptake and interaction.

Both calcium alginate beads and NP-ABs exhibit type V physisorption isotherm, which shows weak interactions between adsorbent and adsorbate and is obtained with certain porous materials [33].

The morphology of the 1% NP-ABs was determined by Scanning Electron Microscopy and the images of the NP-ABs are shown in Figure 2. The images show a microporous structure with particles embedded within the NP-ABs.
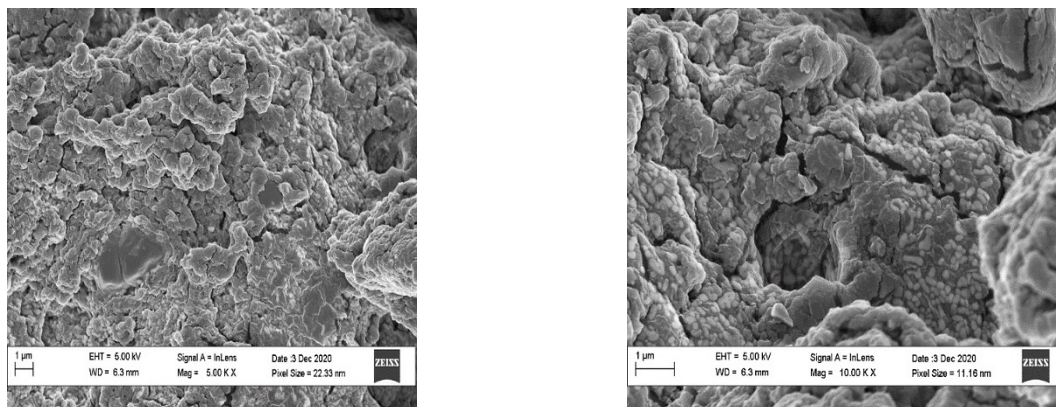
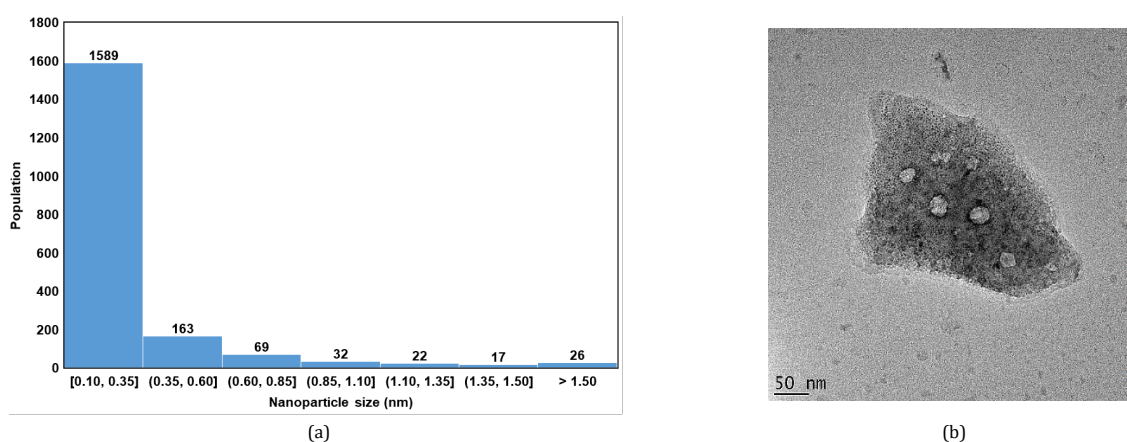**Figure 2.** Scanning Electron Micrograph images of the NP-ABs.

(a)

(b)

Figure 3. (a) Particle size distribution and (b) Transmission Electron Micrograph of the P-ZrO$_2$CeO$_2$ZnO nanoparticles.
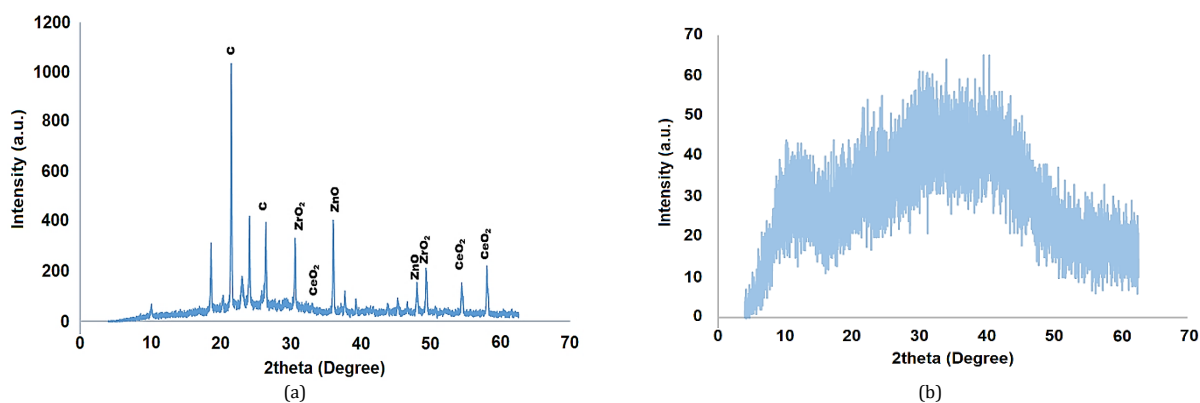

(a)

(b)

Figure 4. XRD diffraction pattern of (a) P-ZrO$_2$CeO$_2$ZnO nanoparticles and (b) NP-ABs.

The morphology and particle size distribution of the P-ZrO$_2$CeO$_2$ZnO nanoparticles that were incorporated into the NP-ABs were determined by Transmission Electron microscopy as shown in Figure 3. Figure 3a demonstrates that the size of P-ZrO$_2$CeO$_2$ZnO nanoparticles ranged from 0.10 to 4.53 nm with an average size of 0.24 nm and Figure 3b shows that the nanoparticles were widely dispersed with some clusters in some instances.

The crystalline properties of the nanoparticles/beads composite were determined using an X-ray diffractometer and the results are shown in Figure 4. P-ZrO$_2$CeO$_2$ZnO nanoparticles (Figure 5a) were crystalline with characteristic diffraction peaks at 2θ = 30.78, 49.47 and 54.64° indexed to the monoclinic phase of ZrO (Joint Committee on Powder Diffraction Standards

(JCPDS) No: 01-0731523), 33.15 and 58.06° indexed to the face centred cubic structure of CeO (JCPDS No: 34-0394) and the peak at 36.29° indexed to the wurtzite structure of ZnO (JCPDS No: 36-1451). The NP-ABs (Figure 4b) are amorphous in structure because the XRD pattern does not exhibit Bragg peaks.

3.2. Optimization of SPE experiments

Screening of the most significant factors in the removal of As and Cr was carried out using eight experiments according to the multilevel factorial design [34]. The factors selected were flow rate, dosage, sample volume, pH, eluent concentration, and flow rate.

Table 2. Multiple response prediction parameters.

Response	Goal	Lower	Target	Upper		Weight	Importance		
EF$_{As}$	Maximum	0.69	2.17	100		1	1		
EF$_{Cr}$	Maximum	6.88	16.27	100		1	1		
Metal ion	**Solution**	**Flow rate (mL/min)**	**Dosage (mg)**	**Sample volume (mL)**	**pH**	**Eluent concent. (M)**	**Eluent flow rate (rpm)**	**Enrichment factor fit**	**Composite desirability**
As	1	1	10	5	9	2.0	3	2.17	1
Cr	1	1	40	100	9	0.1	1	18.12	1
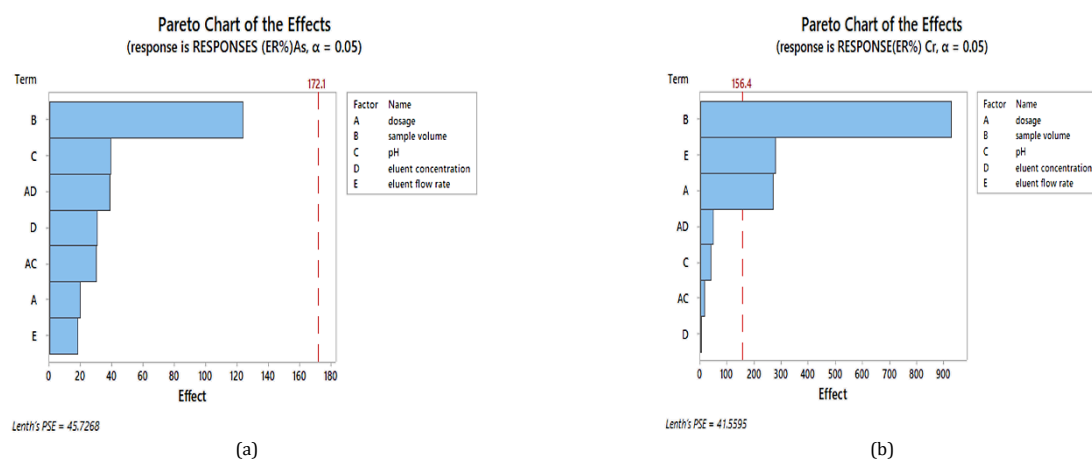
Figure 5. Pareto chart for optimization of the significant effect for solid phase extraction of (a) Cr and (b) As.
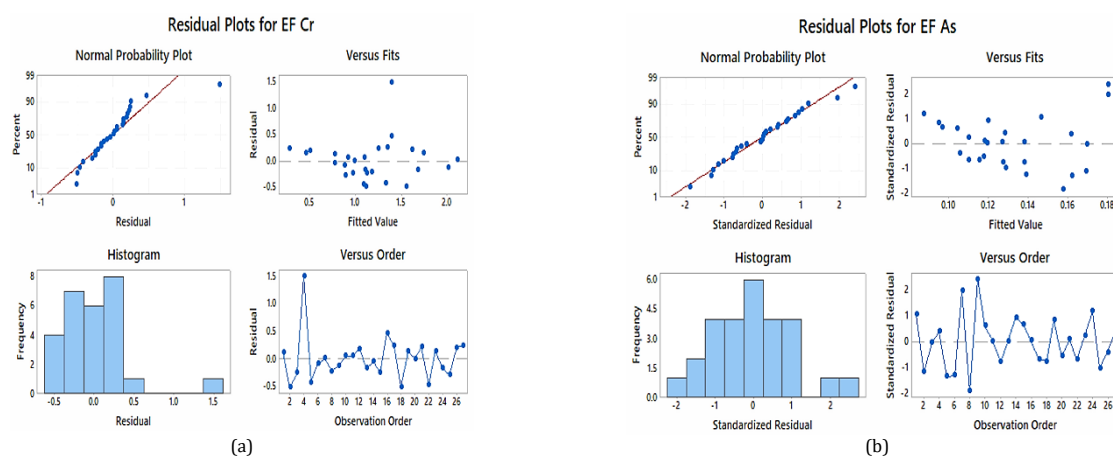
Figure 6. Residual plots for enrichment of (a) Cr and (b) As.

The amount of adsorbent (10, 40 mg), sample volume (5, 100 mL), eluent volume (10 mL), sample pH (3 and 9), eluent flow rate (2 rpm), and eluent concentration 2.0 M were used in the optimization experiments and recovery studies were used to assess extraction efficiency.

The independent factors which were evaluated included sample volume, pH, eluent concentration, eluent flow rate and sample flow rate. A Pareto chart in Figure 5 was used to select the significant variables based on their absolute values, and each value that exceeded the reference determining line was considered a significant variable at the 95% confidence interval. The Pareto chart revealed that sample volume, eluent flow rate, and dosage were the most significant factors for the removal of Cr. For subsequent experiments, the significant variables were considered for optimization using the full factorial design, and the others were fixed [35].

3.3. Optimisation of significant extraction conditions for As and Cr using full factorial design and response surface methodology

The optimization of the screened significant variables (Sample volume, dosage, and eluent flow rate) was carried out using a full factorial design in 21 runs. The residual plots of the optimization process are shown in Figure 6 and the points are scattered around the centre indicating the appropriateness of the model.

The optimum conditions chosen for the experiment that gave favourable results for both metal ions were sample volume 5 mL, dosage 40 mg, pH = 7 and eluent flow rate 1 mL/min and were close to the predicted values in Table 2.

The proposed model to predict the EF of As and Cr is shown in Equations (4) and (5), respectively. A positive value indicates enhancement of the relationship among responses, and a negative value indicates nonenhancement between the responses among the terms.

$$EF_{As} = 0.1510 - 0.000327 \times S - 0.00457 \times D + 0.0092 \times P + 0.000008 \times S \times S + 0.000057 \times D \times D - 0.00092 \times P \times P - 0.000017 \times S \times D - 0.000103 \times S \times P + 0.000469 \times D \times P \quad (4)$$
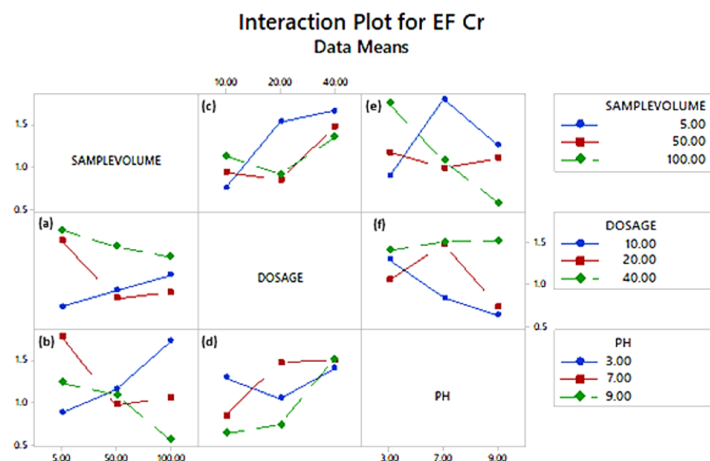
Figure 7. Interaction plots for the effect of sample volume, dosage, and pH on Cr enrichment factors.
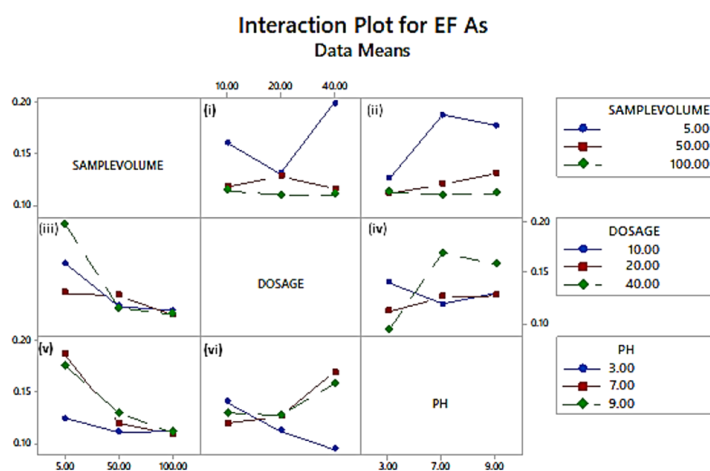

Figure 8. Interaction plots for the effect of sample volume, dosage, and pH on As enrichment factors.

$$EF_{Cr} = -0.080 + 0.0143 \times S - 0.0038 \times D + 0.327 \times P + 0.000062 \times S \times S + 0.00011 \times D \times D - 0.0268 \times P \times P - 0.000185 \times S \times D - 0.002907 \times S \times P + 0.00411 \times D \times P$$

<div align="right">(5)</div>

where S, sample volume; D, dosage; P, pH.

3.4. Interaction between influencing factors and the effects of dosage, pH, and sample volume on enrichment factor

The interaction between the variables was determined using interaction plots. Interactions occur when plots cross each. The interaction plots for Cr are shown in Figure 7. Interactions between sample volume and dosage were observed at 50 mL sample volume (Figure 7a), 12-15 mg of sorbent dosage (Figure 7c). Interaction between sample volume and pH occurred between 40-60 mL sample volume (Figure 7b) and at pH 4 and 7 (Figure 7e). Interactions between dosage and pH were observed at dosage 15 mg and above 35 mg (Figure 7d) as well as at pH 4 and 5 (Figure 7f).

The interactions for As between sorbent dosage and sample volume were observed at 10, 20 and 40 mg of sorbent dosage (Figure 8i) and for sample volume between 40 and 50 mL and above 80 mL (Figure 8iii). Interactions between the sample volume and pH occurred between 10-40 mL and 100 mL (Figure 8v) as well as below pH = 4 (Figure 8ii). The same interactions were observed for *As* at sorbent dosage 15, 20-30 mg (Figure 8vii) as well as between pH = 4-6 and above pH = 8 (Figure 8iv). All regions in which interactions occurred are not

suitable to be used as optimum conditions since the results are affected by various factors which interact.

3.5. Evaluation of the main effects of factors on recovery

The main effects of sample volume, dosage, and pH on the enrichment of As and Cr were determined using Minitab and the results are shown in Figure 9.

The degree of acidity or basicity plays an important role in the uptake of metal ions. When pH was increased from 3 to 9, a general increase on Enrichment factor was observed for both As and Cr, however after pH = 7 a general decline was observed up to pH = 9 for Cr and for As the mean response almost levelled off. Hence, in this study, pH = 7 was selected as the optimum pH for enrichment. Similar quantitative recoveries for Cr(III) were obtained in a similar pH range of 6-8 using *Phallus impudicus* loaded with γ-Fe₂O₃ [36]. The hydroxyl groups on the sorbent are mainly responsible for sample uptake. The groups retain anions under acidic conditions and under basic conditions they retain cations as shown by a study on speciation of arsenic and chromium [37].

Increase in sorbent dosage from 10 to 40 mg resulted in a general increase in the enrichment factor for both As and Cr. Cr showed a higher response to the increase in dosage than As because maybe the sorbate preferentially enriched Cr or the eluent desorbed it preferentially than As. At low sorbent dosage, a lot of the metal ions remain in the solution because the enrichment sites become saturated more quickly.
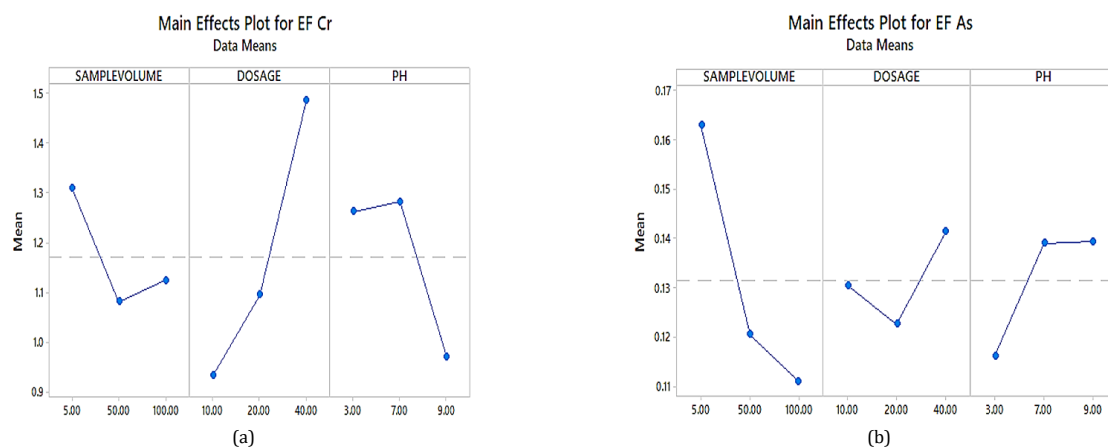
Figure 9. Main effects plots for sample volume, dosage and pH on (a) Cr and (b) As enrichment factor.
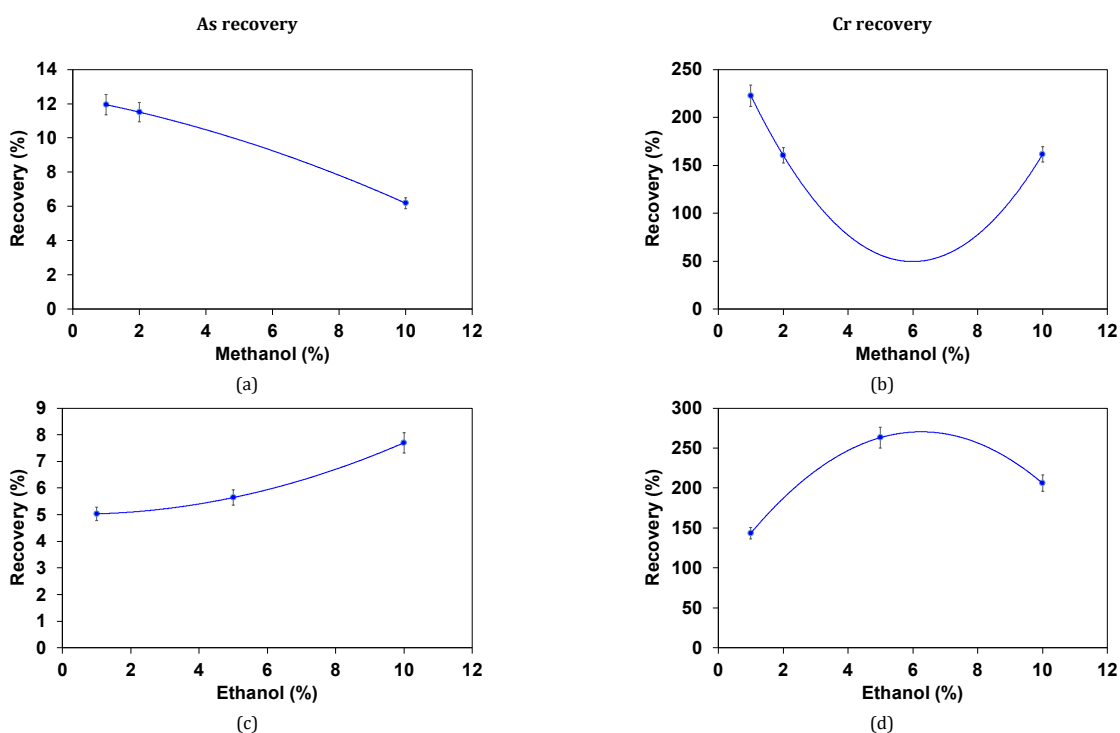

Figure 10. Effect of (a, b) methanol and (c, d) ethanol on the recovery of As and Cr, respectively.

At higher sorbent dosage, the enrichment factor increases because more free active sites are available for uptake of the metal ions. A similar trend was observed for the recovery of Cr and it was concluded that the development was due to an increase in surface area and an accessible site for the adsorption of analytes [38].

The parameter which can influence the extraction efficiency is the sample volume. Generally, a decrease in the enrichment factor was observed for an increase in the sample volume from 5 to 100 mL during the experiment. During other studies a similar trend was noted when they enriched As [39].

3.6. Effect of interference on recovery

Alcohols were evaluated as model organic interferences on the recovery of trace metals, and the results are shown in Figure 10. The effect of alcohols on the extraction of As and Cr solid phases was determined by varying the alcohol concentration from 1, 2, and 10 % ethanol and 1, 5, and 10 % methanol at pH

= 7.0. The dosage of NP-ABs was 20 mg and the concentration of As and Cr was 10 µg/L, the sample volume and eluent were 10 mL.

An increase in the methanol concentration depressed the recovery of As and Cr, while an increase in the ethanol concentration resulted in an increase in the recovery of As; however, an increase in the ethanol concentration resulted in an increase in the recovery of Cr up to 5% and then the recovery was depressed at higher ethanol concentrations in the water samples.

### 3.7. Desorption cycles for solid-phase extraction of As and Cr

To assess the possibility of reusability and regeneration of the adsorbent, the adsorption desorption cycles were carried out and the results are shown in Figure 11. The recovery of As was almost constant for the desorption cycles; however, for Cr recoveries dropped from 102 to 39% during the second cycle and at the fourth cycle it was at 19%.

Table 3. Results of the validation data for the analysis.

Parameter	Cr	As
Range of linearity	0-1000 μg/L	0-1000 μg/L
LOD	8.38×10^{-5} μg/L	4.396×10^{-4} μg/L
LOQ	2.793×10^{-4} μg/L	1.465×10^{-3} μg/L
R^2	0.9999	1.0000
Precision	4.78	0.18
Recovery (EF), %	46.56-130.65	20.96-82.51

Table 4. Results of the recovery test of well and effluent water samples.

Metal ion	Well water				Effluent water			
	Added (μg/L)	Found (μg/L)	Recovery (%)	Preconcentration factor	Added (μg/L)	Found (μg/L)	Recovery (%)	Preconcentration factor
Cr	0.00	0.37±0.14	-	-	0.00	1.11±1.63	-	-
	2.00	1.84±0.07	73.92	1.08	2.00	3.72±0.02	130.65	0.53
	5.00	5.58±0.19	104.38	0.89	5.00	4.8±10.10	74.07	1.04
	10.00	6.54±0.16	61.76	1.52	10.00	5.77±0.06	46.56	1.73
As	0.00	0.13±0.03	-	-	0.00	0.30±0.08	-	-
	2.00	1.05±0.04	45.94	1.90	2.00	1.95±0.04	82.51	1.02
	5.00	2.30±0.07	43.31	2.17	5.00	2.25±0.03	39.04	2.22
	10.00	2.93±0.02	27.96	3.41	10.00	2.40±0.03	20.96	4.17
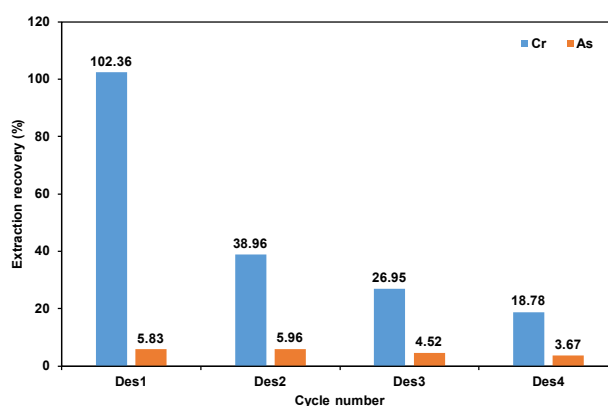
Figure 11. Adsorption desorption cycles for As and Cr.

3.8. Analytical performance

Linearity was determined by calibrations over a range of six standards ranging from 0, 31.25, 62.5, 125, 250, 500, and 1000 μg/L. The calibration points were fitted to linear regression. A sample spiked with standards was analyzed to confirm that the selected regression and linearity are appropriate. The precision of the method (repeatability) was determined by five extractions of 20 μg/L As and Cr using the P-ZrO₂CeO₂ZnO nanoparticle/alginate beads and calculating the relative standard deviation. Repeatability was determined by analysing a single analytical run in a single day, respectively, to determine the precision as relative standard deviation RSD %. The limit of detection (LOD) is defined as $3S_b/m$ and the limit of quantification LOQ defined as $10S_b/m$, where S_b is the standard deviation of the blank signals and m is the slope of calibration curve. The results for the validation data for the analysis are shown in Table 3.

3.9 Application in real samples

Accuracy was determined by carrying out addition recovery experiments for As and Cr in two by spiking real samples from effluent water and well water as shown in Table 4. Spiking was done at three different levels, ie 2.0, 5.0, and 10.0 μg/L As (V) and Cr. Recovery was calculated as % of the difference between the concentration of the analyte of the spiked sample and the concentration of the analyte in the unspiked sample divided by the amount of the standard spiked as shown in Equation (6).

$$\text{Recovery \%} = \frac{C_S - C_0}{s} \times 100 \qquad (6)$$

where C_s: concentration of analyte in spiked sample, C_0: concentration of analyte in unspiked sample and s: the amount of standard spiked.

4. Conclusions

Novel P-ZrO₂CeO₂ZnO NP-ABs were successfully fabricated and characterized. The most significant factors were screened for using a half factorial design and the number of factors was reduced from five to three, namely sample volume, dosage, and eluent flow rate. The selected significant factors were then successfully optimized using a full factorial design and the favourable conditions were sample volume 5 mL, dosage 40 mg and eluent flow rate 1 mL/min. Interactions were observed between sample volume and dosage, sample volume and pH, dosage and pH. This study showed that a preliminary screening step for the most significant factors for As and Cr enrichment helps reduce the number of total runs, and for the same experiment interactions between factors were present, and hence it is necessary to take this into account during the experimental design.

Acknowledgements

Disclosure statement DS

Conflict of interest: The authors declare that they have no conflict of interest. Ethical approval: All ethical guidelines have been adhered.

CRediT authorship contribution statement CR

Conceptualization: Nichodimus Hokonya, Courtie Mahamadi, Netayi Muchanyereyi, Timothy Gutu; Methodology: Nichodimus Hokonya; Software: Nichodimus Hokonya; Validation: Nichodimus Hokonya, Courtie Mahamadi, Netayi Muchanyereyi, Timothy Gutu; Formal Analysis: Nichodimus Hokonya, Courtie Mahamadi, Netayi Muchanyereyi, Timothy Gutu; Investigation: Nichodimus Hokonya; Resources: Nichodimus Hokonya, Courtie Mahamadi, Netayi Muchanyereyi, Timothy Gutu; Data Curation: Nichodimus Hokonya, Courtie Mahamadi, Netayi Muchanyereyi, Timothy Gutu; Writing - Original Draft: Nichodimus Hokonya; Writing - Review and Editing: Nichodimus Hokonya, Courtie Mahamadi, Netayi Muchanyereyi, Timothy Gutu; Visualization: Courtie Mahamadi, Netayi Muchanyereyi and Timothy Gutu; Funding acquisition Courtie Mahamadi, Netayi Muchanyereyi and Timothy Gutu: Supervision: Courtie Mahamadi, Netayi Muchanyereyi and Timothy Gutu; Project Administration: Courtie Mahamadi, Netayi Muchanyereyi and Timothy Gutu

ORCID iD and Email ✉

Nichodimus Hokonya
✉ hokonyanichodimus@gmail.com
iD https://orcid.org/0000-0002-6800-5030
Courtie Mahamadi
✉ cmahamadi@buse.ac.zw
iD https://orcid.org/0000-0002-6643-3285
Netai Mukaratirwa-Muchanyereyi
✉ nmuchanyereyi@gmail.com
iD https://orcid.org/0000-0002-2141-9906
Timothy Gutu
✉ tgutu@science.uz.ac.zw
iD https://orcid.org/0000-0001-5989-5011

References

[1]. Rasool, A.; Farooqi, A.; Xiao, T.; Masood, S.; Kamran, M. A.; Bibi, S. Elevated levels of arsenic and trace metals in drinking water of Tehsil Mailsi, Punjab, Pakistan. *J. Geochem. Explor.* **2016**, *169*, 89–99.

[2]. Raj, K.; Sardar, U. R.; Bhargavi, E.; Devi, I.; Bhunia, B.; Tiwari, O. N. Advances in exopolysaccharides based bioremediation of heavy metals in soil and water: A critical review. *Carbohydr. Polym.* **2018**, *199*, 353–364.

[3]. Genthe, B.; Kapwata, T.; Le Roux, W.; Chamier, J.; Wright, C. Y. The reach of human health risks associated with metals/metalloids in water and vegetables along a contaminated river catchment: South Africa and Mozambique. *Chemosphere* **2018**, *199*, 1–9.

[4]. Singh, R.; Singh, S.; Parihar, P.; Singh, V. P.; Prasad, S. M. Arsenic contamination, consequences and remediation techniques: a review. *Ecotoxicol. Environ. Saf.* **2015**, *112*, 247–270.

[5]. Masindi, V.; Gitari, W. M. Removal of arsenic from wastewaters by cryptocrystalline magnesite: complimenting experimental results with modelling. *J. Clean. Prod.* **2016**, *113*, 318–324.

[6]. Amran, M. B.; Aminah, S.; Rusli, H.; Buchari, B. Bentonite-based functional material as preconcentration system for determination of chromium species in water by flow injection analysis technique. *Heliyon* **2020**, *6*, e04051.

[7]. Yao, L.; Zhu, Y.; Xu, W.; Wang, H.; Wang, X.; Zhang, J.; Liu, H.; Lin, C. Combination of dispersive solid phase extraction with dispersive liquid–liquid microextraction for the sequential speciation and preconcentration of Cr(III) and Cr(VI) in water samples prior to graphite furnace atomic absorption spectrometry determination. *J. Ind. Eng. Chem.* **2019**, *72*, 189–195.

[8]. Sahayam, A. C.; Venkateswarlu, G.; Chaurasia, S. C. Determination of Cr(VI) in potable water samples after selective preconcentration on oxalate form of Dowex-1 and electro thermal atomic absorption spectrometric determination. *Anal. Chim. Acta* **2005**, *537*, 267–270.

[9]. Ahsan, M. A.; Katla, S. K.; Islam, M. T.; Hernandez-Viezcas, J. A.; Martinez, L. M.; Díaz-Moreno, C. A.; Lopez, J.; Singamaneni, S. R.; Banuelos, J.; Gardea-Torresdey, J.; Noveron, J. C. Adsorptive removal of methylene blue, tetracycline and Cr(VI) from water using sulfonated tea waste. *Environ. technol. innov.* **2018**, *11*, 23–40.

[10]. Akhtar, A.; Kazi, T. G.; Afridi, H. I.; Baig, J. A.; Khan, M. Simultaneous preconcentration of toxic elements in eye makeup products through single drop ionic liquid based non-dispersive microextraction method

using narrow glass column: Multivariate application. *Microchem. J.* **2020**, *157*, 104963.

[11]. Molaei, K.; Bagheri, H.; Asgharinezhad, A. A.; Ebrahimzadeh, H.; Shamsipur, M. SiO 2 -coated magnetic graphene oxide modified with polypyrrole–polythiophene: A novel and efficient nanocomposite for solid phase extraction of trace amounts of heavy metals. *Talanta* **2017**, *167*, 607–616.

[12]. Yavuz, E.; Tokalıoğlu, Ş.; Şahan, H.; Patat, Ş. Nanosized spongelike Mn3O4 as an adsorbent for preconcentration by vortex assisted solid phase extraction of copper and lead in various food and herb samples. *Food Chem.* **2016**, *194*, 463–469.

[13]. Mandlate, J. S.; Soares, B. M.; Seeger, T. S.; Vecchia, P. D.; Mello, P. A.; Flores, E. M. M.; Duarte, F. A. Determination of cadmium and lead at sub-ppt level in soft drinks: An efficient combination between dispersive liquid-liquid microextraction and graphite furnace atomic absorption spectrometry. *Food Chem.* **2017**, *221*, 907–912.

[14]. Özzeybek, G.; Şahin, İ.; Erarpat, S.; Bakirdere, S. Reverse phase dispersive liquid–liquid microextraction coupled to slotted quartz tube flame atomic absorption spectrometry as a new analytical strategy for trace determination of cadmium in fish and olive oil samples. *J. Food Compost. Anal.* **2020**, *90*, 103486.

[15]. Blanchet-Chouinard, G.; Larivière, D. Determination of Pb in environmental samples after cloud point extraction using crown ether. *Talanta* **2018**, *179*, 300–306.

[16]. Arslan, Z.; Oymak, T.; White, J. Triethylamine-assisted Mg(OH)2 coprecipitation/preconcentration for determination of trace metals and rare earth elements in seawater by inductively coupled plasma mass spectrometry (ICP-MS). *Anal. Chim. Acta* **2018**, *1008*, 18–28.

[17]. Kim, E. J.; Baek, K. Enhanced reductive extraction of arsenic from contaminated soils by a combination of dithionite and oxalate. *J. Hazard. Mater.* **2015**, *284*, 19–26.

[18]. Najafi, N. M.; Eidizadeh, M.; Seidi, S.; Ghasemi, E.; Alizadeh, R. Developing electrodeposition techniques for preconcentration of ultra-traces of Ni, Cr and Pb prior to arc-atomic emission spectrometry determination. *Microchem. J.* **2009**, *93*, 159–163.

[19]. Płotka-Wasylka, J.; Szczepańska, N.; Owczarek, K.; Namieśnik, J. Miniaturized Solid Phase Extraction. In *Comprehensive Analytical Chemistry*; Elsevier, 2017; pp. 279–318.

[20]. Calderilla, C.; Maya, F.; Leal, L. O.; Cerdà, V. Recent advances in flow-based automated solid-phase extraction. *Trends Analyt. Chem.* **2018**, *108*, 370–380.

[21]. Dimpe, K. M.; Ngila, J. C.; Nomngongo, P. N. Preparation and application of a tyre-based activated carbon solid phase extraction of heavy metals in wastewater samples. *Phys. Chem. Earth (2002)* **2018**, *105*, 161–169.

[22]. Chen, S.; Wang, C.; Yan, J.; Lu, D. Use of fibrous TiO2@graphitic carbon nitride nanocomposites in dispersive micro-solid phase extraction for arsenic species before inductively coupled plasma mass spectrometry determination. *Microchem. J.* **2020**, *158*, 105211.

[23]. Ghazaghi, M.; Mousavi, H. Z.; Rashidi, A. M.; Shirkhanloo, H.; Rahighi, R. Graphene-silica hybrid in efficient preconcentration of heavy metal ions via novel single-step method of moderate centrifugation-assisted dispersive micro solid phase extraction. *Talanta* **2016**, *150*, 476–484.

[24]. Barciela-Alonso, M. C.; Plata-García, V.; Rouco-López, A.; Moreda-Piñeiro, A.; Bermejo-Barrera, P. Ionic imprinted polymer based solid phase extraction for cadmium and lead pre-concentration/determination in seafood. *Microchem. J.* **2014**, *114*, 106–110.

[25]. He, M.; Huang, L.; Zhao, B.; Chen, B.; Hu, B. Advanced functional materials in solid phase extraction for ICP-MS determination of trace elements and their species - A review. *Anal. Chim. Acta* **2017**, *973*, 1–24.

[26]. Alipanahpour Dil, E.; Ghaedi, M.; Asfaram, A.; Mehrabi, F.; Bazrafshan, A. A. Optimization of process parameters for determination of trace Hazardous dyes from industrial wastewaters based on nanostructures materials under ultrasound energy. *Ultrason. Sonochem.* **2018**, *40*, 238–248.

[27]. Asfaram, A.; Ghaedi, M.; Goudarzi, A. Optimization of ultrasound-assisted dispersive solid-phase microextraction based on nanoparticles followed by spectrophotometry for the simultaneous determination of dyes using experimental design. *Ultrason. Sonochem.* **2016**, *32*, 407–417.

[28]. Jain, A.; Wadhawan, S.; Kumar, V.; Mehta, S. K. Colorimetric sensing of Fe3+ ions in aqueous solution using magnesium oxide nanoparticles synthesized using green approach. *Chem. Phys. Lett.* **2018**, *706*, 53–61.

[29]. Sharma, J.; Bhogal, S.; Naushad, M.; Inamuddin; Kumar, A.; Stadler, F. J. Microwave assisted fabrication of La/Cu/Zr/carbon dots trimetallic nanocomposites with their adsorptional vs photocatalytic efficiency for remediation of persistent organic pollutants. *J. Photochem. Photobiol. A Chem.* **2017**, *347*, 235–243.

[30]. Bayat, M.; Javanbakht, V.; Esmaili, J. Synthesis of zeolite/nickel ferrite/sodium alginate bionanocomposite via a co-precipitation technique for efficient removal of water-soluble methylene blue dye. *Int. J. Biol. Macromol.* **2018**, *116*, 607–619.

[31]. Shah, J.; Kumar Kotnala, R. Rapid green synthesis of ZnO nanoparticles using a hydroelectric cell without an electrolyte. *J. Phys. Chem. Solids* **2017**, *108*, 15–20.

[32]. Gnanamoorthi, K.; Balakrishnan, M.; Mariappan, R.; Ranjith Kumar, E. Effect of Ce doping on microstructural, morphological and optical properties of ZrO2 nanoparticles. *Mater. Sci. Semicond. Process.* **2015**, *30*, 518–526.

[33]. Thommes, M.; Kaneko, K.; Neimark, A. V.; Olivier, J. P.; Rodriguez-Reinoso, F.; Rouquerol, J.; Sing, K. S. W. Physisorption of gases, with special reference to the evaluation of surface area and pore size distribution (IUPAC Technical Report). *Pure Appl. Chem.* **2015**, *87*, 1051–1069.

[34]. Khazaeli, E.; Haddadi, H.; Zargar, B.; Hatamie, A. Response surface methodology based on central composite design as a chemometric tool for optimizing dispersive liquid–liquid microextraction for determining ultra-trace amounts of zinc in oil and water samples. *Anal. Methods* **2016**, *8*, 5101–5110.

[35]. Abbaspour, M.; Makhmalzadeh, B. S.; Arastoo, Z.; Jahangiri, A.; Shiralipour, R. Effect of anionic polymers on drug loading and release

from clindamycin phosphate solid lipid nanoparticles. *Trop. J. Pharm. Res.* **2013**, *12*, 477–482.

[36]. Serkan Yalçın, M.; Kılınç, E.; Özdemir, S.; Yüksel, U.; Soylak, M. Phallus impudicus loaded with γ-Fe2O3 as solid phase bioextractor for the preconcentrations of Zn(II) and Cr(III) from water and food samples. *Process Biochem.* **2020**, *92*, 149–155.

[37]. Baranik, A.; Gagor, A.; Queralt, I.; Marguí, E.; Sitko, R.; Zawisza, B. Determination and speciation of ultratrace arsenic and chromium species using aluminium oxide supported on graphene oxide. *Talanta* **2018**, *185*, 264–274.

[38]. Ghorbani, Y. A.; Ghoreishi, S. M.; Ghani, M. Derived N-doped carbon through core-shell structured metal-organic frameworks as a novel sorbent for dispersive solid phase extraction of Cr(III) and Pb(II) from water samples followed by quantitation through flame atomic absorption spectrometry. *Microchem. J.* **2020**, *155*, 104786.

[39]. Zhang, Y.; Wang, W.; Li, L.; Huang, Y.; Cao, J. Eggshell membrane-based solid-phase extraction combined with hydride generation atomic fluorescence spectrometry for trace arsenic(V) in environmental water samples. *Talanta* **2010**, *80*, 1907–1912.